JACS
JOURNAL OF THE AMERICAN CHEMICAL SOCIETY

Article

pubs.acs.org/JACS

Achieving Selective and Efficient Electrocatalytic Activity for CO_2 Reduction Using Immobilized Silver Nanoparticles

Cheonghee Kim,[†,▽] Hyo Sang Jeon,[†,‡,▽] Taedaehyeong Eom,[§] Michael Shincheon Jee,[†,∥] Hyungjun Kim,[§] Cynthia M. Friend,[⊥] Byoung Koun Min,[*,†,‡,#] and Yun Jeong Hwang[*,†,‡]

[†]Clean Energy Research Center, Korea Institute of Science and Technology, Seoul 02792, Republic of Korea

[‡]Korea University of Science and Technology, Daejeon 34113, Republic of Korea

[§]Graduate School of Energy, Environment, Water, and Sustainability (EEWS), Korea Advanced Institute of Science and Technology (KAIST), Daejeon, 34141, Republic of Korea

[∥]Department of Chemical and Biological Engineering, Korea University, Seoul 02841, Republic of Korea

[⊥]Department of Chemistry and Chemical Biology, Harvard University, Cambridge, Massachusetts 02138, United States

[#]Green School, Korea University, Seoul 02841, Republic of Korea

Supporting Information

ABSTRACT: Selective electrochemical reduction of CO_2 is one of the most sought-after processes because of the potential to convert a harmful greenhouse gas to a useful chemical. We have discovered that immobilized Ag nanoparticles supported on carbon exhibit enhanced Faradaic efficiency and a lower overpotential for selective reduction of CO_2 to CO. These electrocatalysts were synthesized directly on the carbon support by a facile one-pot method using a cysteamine anchoring agent resulting in controlled monodispersed particle sizes. These synthesized Ag/C electrodes showed improved activities, specifically decrease of the overpotential by 300 mV at 1 mA/cm^2, and 4-fold enhanced CO Faradaic efficiency at −0.75 V vs RHE with the optimal particle size of 5 nm compared to polycrystalline Ag foil. DFT calculations enlightened that the specific interaction between Ag nanoparticle and the anchoring agents modified the catalyst surface to have a selectively higher affinity to the intermediate COOH over CO, which effectively lowers the overpotential.

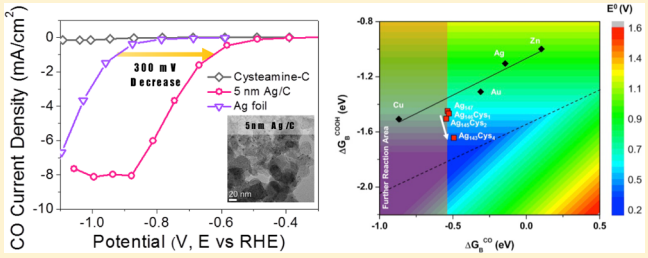

INTRODUCTION

Atmospheric concentrations of carbon dioxide, a greenhouse gas, are ever increasing due to the continued use of traditional fossil fuels, leading to adverse global climate.[1,2] In an effort to mitigate the worldwide dependence on fossil fuels and, thus, CO_2 emission, there is increasing emphasis on the development of renewable energy sources, and as a more active response, conversion of carbon dioxide to a reusable carbon form, a sustainable carbon recycling system, has been suggested.[3,4] Among various methods for CO_2 conversion, electrochemical CO_2 reduction in aqueous solution has attracted considerable attention since it is environmentally clean and can be combined with renewable energy resources such as solar and wind energies to store them in the form of chemical energy.[5] However, electrochemical CO_2 reduction reaction suffers from poor efficiency for several reasons, including the requirement of a large overpotential, difficulty in controlling selectivity, and competition with hydrogen evolution reaction in aqueous environment.[6] Therefore, it is necessary and important to design a new catalyst with high efficiency and selectivity.

Gold, silver, and copper have been identified as promising CO_2 reduction reaction electrocatalysts[7] because CO (*CO) relatively weakly binds on their surfaces compared to hydrogen evolution electrocatalysts such as platinum. Especially, Au and Ag had been reported to have highly selective conversions from CO_2 to CO in electrochemical CO_2 reduction reaction, while Cu produces a mixture of more reduced form of hydrocarbon products such as CH_4, C_2H_4, ethanol, etc. Although Ag shows as great selectivity as Au but cheaper cost, Ag has not been widely studied[8] because the required overpotential is larger than Au. Many of the Ag-based electrocatalysts have been studied in nonaqueous electrolyte such as ionic-liquids.[9] Recently, density functional theory (DFT) calculation reported that Ag-based catalysts doped by S or As can decrease the overpotential for CO_2 to CO electrochemical conversion,[10] which motivates the development of Ag-based electrocatalysts for CO_2 reduction reaction.

Recently, the surfaces of bulk polycrystalline metals have been modified to form nanostructures in order to improve catalytic activity for CO_2 reduction reaction. For example, oxide-derived Au nanoparticles or Ag nanoporous demonstrated low overpotentials and high stability for CO production, where high-index facets of the curved surfaces were suggested

Received: June 24, 2015
Published: October 8, 2015

DOI: 10.1021/jacs.5b06568
J. Am. Chem. Soc. 2015, 137, 13844−13850

to be related to high activity.[11,12] In addition, the size effect of nanoparticles associated with changes in the ratio between the edge and corner sites has been demonstrated with Au and Cu metals[13,14] in the aqueous electrolyte. Zhu et al. proposed that edge sites of Au nanoparticles prefer CO evolution, whereas corner sites are active for the competitive H_2 evolution.[13,15] Therefore, the existence of the optimal particle size has been suggested for the CO_2 reduction reaction with high activity and selectivity. Because the prevalence of high-index facets or edge sites varies as the morphology and the size of the nanoparticle changes, uniform synthesis is important to understand nanomorphology influence on the CO_2 reduction reaction activity.

Wet chemistry synthesis allows metallic nanoparticles with uniformly controlled sizes and shapes that can easily be obtained in large quantities.[16−19] To use them for electrocatalysts, they have been deposited on a carbon support of a high surface area after the nanoparticle synthesis as a two-step process. An alternative and more advantages approach for electrocatalytic applications is the direct growth of nanoparticles on the carbon supports with anchoring agents. The anchoring agent acts a role of nucleating sites that induce monodisperse particle synthesis and immobilize on the support simultaneously.[20,21]

In this study, we developed a direct one-pot synthesis of Ag nanoparticles on carbon support using an anchoring agent (cysteamine) and successfully controlled uniform particle sizes. Three different sized silver particles (3, 5, and 10 nm) supported on carbon (nanosized Ag/C) were evaluated for electrochemical CO_2 reduction reaction in an aqueous environment, and the influence of the anchoring agent on the CO_2 reduction activity was investigated. Particles with a diameter of 5 nm showed a high activity, enhanced durability, and maximum Faradaic efficiency (84.4%) for the CO_2 to CO electrochemical conversion. Notably, the overpotential for CO production had reduced about 300 mV at 1 mA/cm^2 with 5 nm sized Ag/C when compared with polycrystalline Ag foil. We propose that the anchoring agent modifies the spatial spin density of the Ag nanoparticles, which decreases the overpotential for CO_2 to CO reduction by DFT calculations.

RESULTS AND DISCUSSION

Immobilized Ag Nanoparticle Synthesis with an Anchoring Agent. Ag nanoparticles of three different sizes were easily synthesized by using a Ag precursor, carbon black, and cysteamine. The size of the Ag nanoparticles was 3.4 ± 0.6 nm when synthesized at 160 °C for 1 h (denoted as 3 nm Ag/C), 5.0 ± 0.9 nm at 160 °C for 3 h (denoted as 5 nm Ag/C) and 10.6 ± 2.8 nm at 200 °C for 1 h (denoted as 10 nm Ag/C) as shown in Figure 1a−c. A high resolution transmission electron microscopy (HR-TEM) image confirmed the single crystalline Ag nanoparticles with a *d*-spacing of 0.23 nm, which corresponds to the (111) crystal plane of face-centered cubic silver (Figure 1d). Further, the X-ray diffraction (XRD) data in Figure S1 show that these nanoparticles are face-centered cubic Ag crystal structure. Without cysteamine, we found that, from TEM images (Figure 1 and Figure S2), Ag particles cannot be directly grown on the carbon support and the sizes of the nanoparticles were not controlled because cysteamine molecules helps to anchor nanoparticles in the initial nucleation step.[20,21]

To investigate the role of cysteamine, X-ray photoelectron spectroscopy (XPS) was conducted on the carbon black,

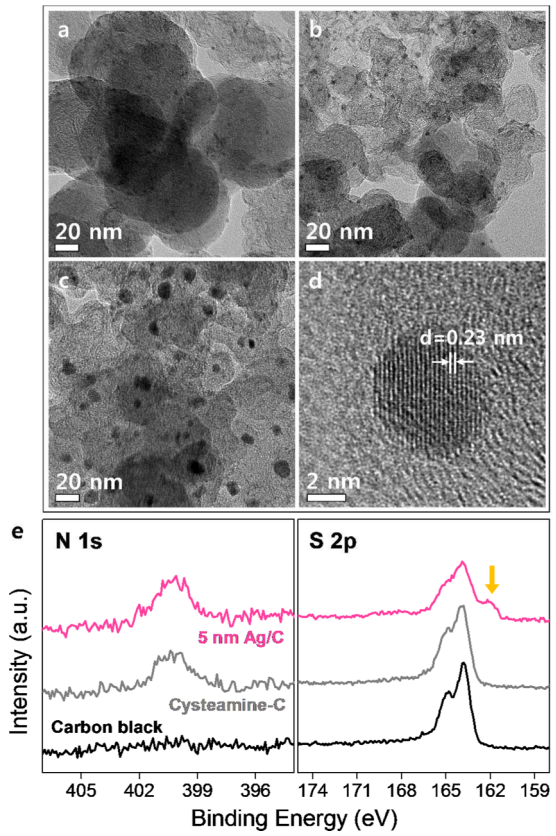

Figure 1. TEM image of (a) 3 nm, (b) 5 nm and (c) 10 nm sized Ag nanoparticles directly synthesized on carbon support. (d) HR-TEM image of 5 nm Ag/C, and (e) XPS spectra of 5 nm Ag/C, Cysteamine-C and Carbon black for N 1s and S 2p.

cysteamine treated carbon (denoted as Cysteamine-C) and prepared Ag nanoparticles/C (Figure 1e and Figure S3a). Figure 1e shows a clear N 1s peak for the Cysteamine-C and 5 nm Ag/C while its absence for carbon black indicates that cysteamine was immobilized on the carbon support. On the other hand, Ag/C particles commonly show additional S 2p peaks (see an arrow in Figure 1e, and pink lines in Figure S3a) unlike those of carbon black and Cysteamine-C. The additional S $2p_{3/2}$ peak possesses the binding energy at 162.1 eV, associated with an Ag−S bond[22] which results from the interaction of the cysteamine with the Ag surface. Such interaction affects the electronic structure of Ag where the relative intensity of a minor Ag 3d peak (orange lines in Figure S3b) increases as that of the S $2p_{3/2}$ peak at 162.1 eV increases. Cysteamine amount was estimated by comparing the Ag 3d and S 2p signal in XPS (see Supporting Information). The Ag−S bond ratio of 5 nm Ag/C (22.0%) was observed to be higher than those of 3 nm Ag/C (18.6%) and 10 nm Ag/C (16.3%). The carbon black as purchased also showed S 2p peaks remnant from its production process.[23]

Electrochemical CO_2 Reduction with Nanoparticulated Ag/C and Ag Foil. The electrochemical CO_2 reduction reaction was performed using the prepared 3, 5, and 10 nm Ag/C samples, and all showed enhanced catalytic activity for CO production compared with the polycrystalline Ag foil (Figure 2a and Figure S4). Figure 2a shows the *iR*-corrected potential dependent CO partial current densities, which were measured at the steady-state current density from chronoamperometry. The CO partial current density of 5 nm Ag/C showed highest

DOI: 10.1021/jacs.5b06568
J. Am. Chem. Soc. 2015, 137, 13844−13850

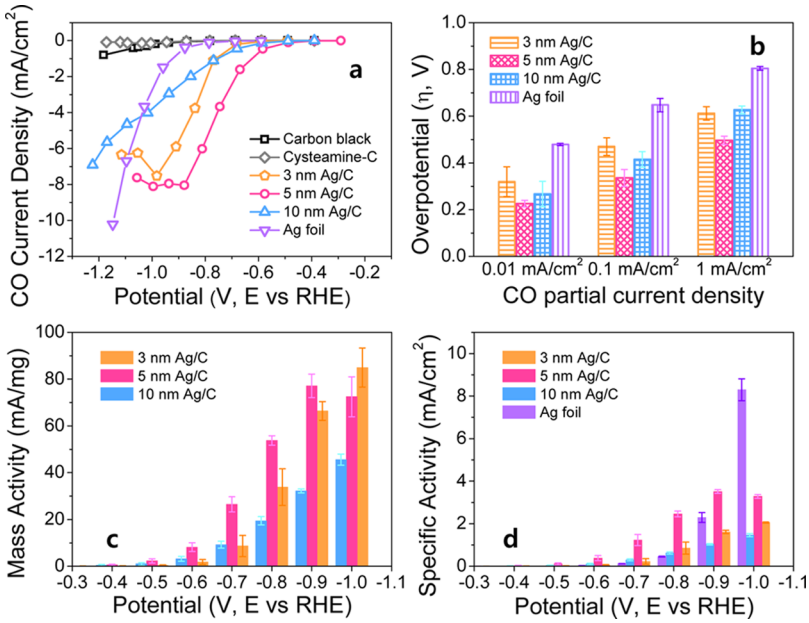

Figure 2. (a) CO partial current density depending on applied potential, (b) overpotentials at fixed current densities, (c) mass activity depending on applied potential and (d) specific activity depending on applied potential. Specific activity was normalized by electrochemically active surface area of silver measured from Pb UPD. CO_2 electrochemical reduction was performed in CO_2-saturated 0.5 M $KHCO_3$. The thermodynamic reduction potential for CO_2 to CO is −0.11 V vs RHE.

values at the low cathodic potential region (−0.3 to −0.9 V vs RHE). Meanwhile, the 3 and 10 nm Ag/C started to show CO partial current density at a higher biased potential region than 5 nm Ag/C, while Ag foil had an even larger cathodic onset potential meaning a larger required overpotentials for CO_2 reduction reaction. Our Ag foil data is well matched with the previous report.[8]

In order to compare the required overpotentials further, we obtained overpotentials at a fixed current density and overpotentials dependent CO partial current density (Figure 2b and Figure S5). The thermodynamic reduction potential for CO_2 to CO is −0.11 V vs RHE. All of the prepared Ag/C samples showed a noticeable decrease in overpotential and 5 nm Ag/C showed the largest diminishment. To be specific, 5 nm Ag/C showed about 300 mV anodic shift of overpotential at 1 mA/cm^2, when compared with Ag foil. Furthermore, as seen in Figure 2c mass activity of three different nanoparticle Ag/C electrodes at various potentials followed a similar trend with CO current density normalized with an electrode area since the amount of Ag metal content was controlled using inductively coupled plasma (ICP) results in all fabricated electrodes. Additionally, the electrochemical surface area (ECSA) of Ag electrode was measured by using an underpotential deposition (UPD) method (Figure S6). The ECSAs of Ag electrodes were 1.8, 1.2, 1.2, and 0.17 cm^2 for 3, 5, 10 nm Ag/C, and Ag foil, respectively. Figure 2d shows specific activities of the Ag electrodes normalized with the measured ECSAs. 5 nm Ag/C has the highest specific activity when compared with that of 3 nm Ag/C, 10 nm Ag/C, and Ag foil before reaching mass transfer limitation of CO_2.

To confirm that the activity for CO_2 reduction of the Ag/C electrodes is induced by the Ag nanoparticles, not by the carbon support itself or Cysteamine-C, CO_2 reduction reactions with both samples were performed under the same condition. Small CO partial current densities were detected for carbon black and Cysteamine-C (Figure 2a) although their total current densities sharply increased as the applied potentials exceeded −0.8 V vs RHE (Figure S7). Identification of the gas products by gas chromatography (GC) measurements confirmed that high amount of hydrogen was generated as the major product when Ag was not loaded on the carbon support. These results indicated that both carbon support and Cysteamine-C were incapable of CO_2 reduction reaction.

The selectivity of CO_2 reduction reaction to CO was also studied with the prepared Ag electrodes by varying the applied potentials (Figure 3a and Figure S8). The enhanced CO production selectivity over hydrogen evolution reaction (HER) was commonly notable at less cathodically biased region with the synthesized Ag/C of three different sizes compared to that

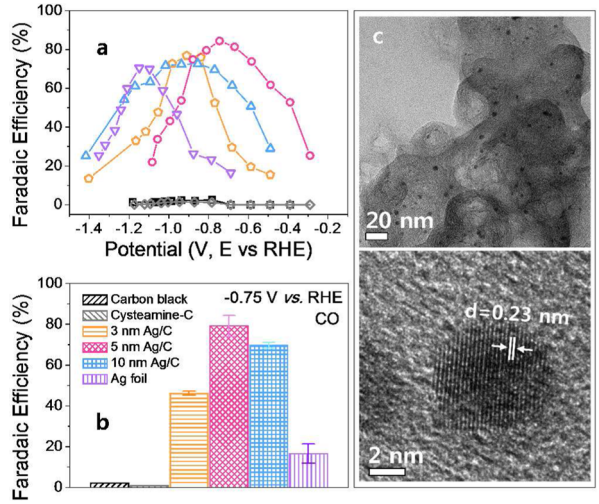

Figure 3. CO Faradaic efficiency (a) depending on applied potential and (b) fixed potential at −0.75 V (vs RHE). CO_2 electrochemical reduction was performed in CO_2-saturated 0.5 M $KHCO_3$. (c) TEM image and HR-TEM image of 5 nm Ag/C after CO_2 reduction.

DOI: 10.1021/jacs.5b06568
J. Am. Chem. Soc. 2015, 137, 13844−13850

of Ag foil. Again, where the 5 nm Ag/C showed the best CO_2 reduction reaction performance reaching its maximum CO Faradaic efficiency with the smallest overpotential (635 mV), and 10 and 3 nm Ag/C, and Ag foil followed sequentially. In addition, the maximum CO Faradaic efficiencies were 76.8, 84.4, 72.6, and 70.5% for 3, 5, 10 nm Ag/C, and Ag foil, respectively, with 5 nm Ag/C achieving the highest CO Faradaic efficiency. When CO Faradaic efficiencies of all samples were compared at a fixed potential of −0.75 V vs RHE, the maximum selectivity potential for 5 nm Ag/C (Figure 3b), Faradaic efficiency of the 5 nm Ag/C (average FE_{CO} = 79.2%) showed 4.8 times enhancement compared to Ag foil (average FE_{CO} = 16.5%). In our study, mass activity, overpotentials, and CO Faradaic efficiency demonstrated that 5 nm was the optimal Ag nanoparticle size for CO_2 reduction reaction application in aqueous solution. Figure S9 shows the Faradaic efficiency of the 5 nm Ag/C for H_2 and CO products in detail. Methane (CH_4) is also one of the gaseous products but less than 1% Faradaic efficiency was detected at all potentials regardless the type of working electrodes. Major products are H_2 and CO, and the sum of their Faradaic efficiencies was close to 100% for each sample according to GC measurements indicating liquid products such as formic acid were negligible, which are consistent with the previous study with Ag foil.[8] Additionally, the TEM and HR-TEM image after CO_2 reduction reaction showed that the 5 nm Ag/C has exhibited no size change and had an average size of 5.0 ± 1.0 nm (Figure 3c).

The 5 nm Ag/C catalyst is the optimum size among the three different nanoparticle sizes even though high surface areas are expected to provide higher activity. Specifically, the 5 nm Ag particles yielded higher current density and selectivity than the 3 nm Ag/C for CO_2 to CO conversion. This size dependency on the selectivity can be understood by the competition of catalytic active sites. For the case of Au nanoparticles, previous study reported that the edge sites can stabilize the intermediate species of the CO_2 reduction reaction more efficiently and also more readily lead to CO evolution compared to corner sites.[13] On the other hand corner sites, which represent a larger fraction of smaller nanoparticles, are more active for HER.[13,15] In our samples, we think that the optimum size of Ag nanoparticle to maximize the selectivity of the CO_2-to-CO reduction reaction was achieved at 5 nm size. This is also in consistent with the previous study performed in an organic electrolyte,[9] which showed that 5 nm Ag nanoparticles had the highest CO partial current density at a given bias potential.

Notably, the reduction of overpotentials with our Ag nanoparticle/C samples relative to Ag foil is also a significant improvement. Beyond the increase of the mass activity as well as the CO Faradaic efficiency with 5 nm Ag/C, we found that the onset potentials for CO_2 reduction reaction (Figure 2) and the overpotentials at the maximum CO Faradaic efficiency (Figure 3) shifted in the anodic direction, both of which indicates the overpotentials for CO production decreased with Ag/C samples.

The 5 nm Ag/C is also more durable than polycrystalline Ag foil (Figure S10). Durability tests were performed with Ag foil and the prepared 5 nm Ag/C at a specific potentials (−1.1 V vs RHE for Ag foil, and −0.8 V vs RHE for 5 nm Ag/C) for 5 h. Although current densities were stable for both Ag foil and the 5 nm Ag/C during 5 h durability test, the decline of the CO Faradaic efficiency was dramatically different. The decline of the CO Faradaic efficiency was 58.2% (from 70.1% to 29.3%) for Ag foil after 5 h. Meanwhile, the CO Faradaic efficiency of 5 nm Ag/C after 5 h decreased only by 18.9% (from 78.3% to 63.5%). When the durability test with Ag foil was performed at −0.8 V vs RHE, a same potential applied to 5 nm Ag/C, the CO Faradaic efficiency decreased from 19.2% to 7.7% within 1 h, and became a HER catalyst. For both samples, the CO Faradaic efficiency loss was transferred to H_2 Faradaic efficiency. Lastly, $^{13}CO_2$ isotope experiment confirmed that the source of C was derived completely from the dissolved CO_2 in aqueous solution (Figure S11), and C from carbon support or cysteamine molecules were not involved in the reduction reaction.

The rate-determining step (RDS) of the CO_2 reduction reaction is generally thought to be formation of an adsorbed CO_2^- ($*CO_2^-$) intermediate on surfaces since the anionic radical is highly unstable. The prepared Ag/C samples and Ag foil had similar Tafel slopes around 140 mV dec^{-1} (Figure S12 and Table S1), which indicates that the CO_2 to $*CO_2^-$ intermediate conversion step requires a large overpotential, and the RDS is not changed for the nanoparticulate Ag/C. However, exchange current densities commonly increased for Ag/C samples and more than 60 times enhancement was obtained with 5 nm Ag/C compared to Ag foil (Table S1). A higher exchange current density implies a higher intrinsic rate of electron transfer between an electrolyte and the electrode and higher catalytic kinetics. Moreover, the CO_2 reduction reaction activities of the previously reported silver-based electrocatalysts are summarized in Table S2. Our cysteamine anchored Ag catalysts showed significantly high mass activity as well.

Understanding Decrease of the Overpotential: The Role of Cysteamine Anchoring Agent. Using DFT calculations, we examined the origin of enhanced catalytic activity of Ag/C. The previous theoretical study on the CO_2 reduction reaction mechanism suggested that the binding energy of the COOH intermediate (ΔE_B^{COOH}) primarily determines the overpotential; higher COOH binding yields lower overpotential.[13,24] We thus calculated ΔE_B^{COOH} to particles of various sizes: 1.0, 1.6, 2.2, and 2.7 nm cuboctahedral Ag nanoparticles (i.e., Wulff shape of Ag), which are Ag_{13}, Ag_{55}, Ag_{147}, and Ag_{309} respectively (Figure 4a). Unsurprisingly, low coordination number (CN) sites exposed at the corners (CN = 5) or edges (CN = 7) strongly bind to COOH. However, the tunability of E_B^{COOH} (that is directly related to the tunability of the overpotential) decreases as the nanoparticle size increases, and becomes only within 126 meV (difference of ΔE_B^{COOH} for CN = 5 and CN = 8) even when the nanoparticle size is 2.7 nm (that is the largest size available within our limited computational cost). This suggests that size effects alone cannot explain the strong overpotential modulation observed from experiments varying the nanoparticle size from 3 to 10 nm. Notably, the previous Ag or Au nanoparticle reports only showed the changes of the CO_2 reduction current densities depending on the particle size, and the onset overpotentials for CO_2 reduction reaction were almost similar regardless of the particle size.[9,13]

Consequently, the low overpotentials with our Ag/C samples are expected to be associated with the anchoring agent, end group of −SH in cysteamine, that can change the electronic structure in Ag surface as confirmed XPS. To investigate this possibility, we performed DFT calculations of 2.2 nm Ag nanoparticle anchored with n number of cysteamine (Cys); $Ag_{(147-n)}Cys_n$ (n = 0, 1, 2, 4) through Ag−S bonds. As shown in Figure 4b, we found E_B^{COOH} shows a monotonic increase as the

DOI: 10.1021/jacs.5b06568
J. Am. Chem. Soc. 2015, 137, 13844−13850

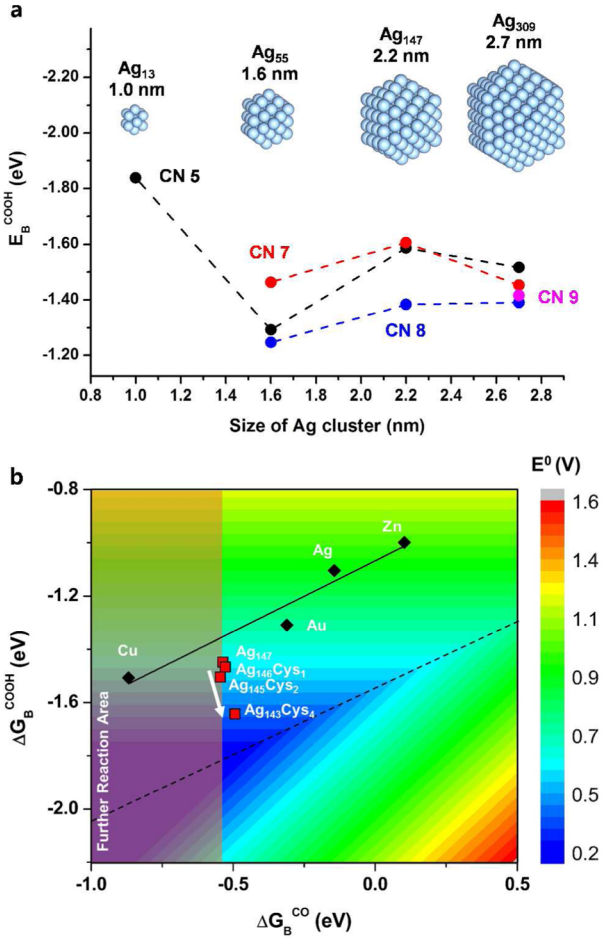

Figure 4. (a) DFT results on the binding energies of the COOH intermediate (ΔE_B^{COOH}) as a function of Ag nanoparticle size. Ag_{13} (1.0 nm), Ag_{55} (1.6 nm), Ag_{147} (2.2 nm), and Ag_{309} (2.7 nm) models with cuboctahedral geometry were examined. (b) Effect of anchoring agents on COOH and CO binding energies examined using $Ag_{(147-n)}Cys_n$ (n = 0,1,2,4) models. Colored map shows the theoretical CO_2 reduction potential (E^0) as a function of COOH and CO binding free energies (ΔG_B^{COOH} and ΔG_B^{CO}; taken from the ref 10). Free energy values of ΔG_B^{COOH} and ΔG_B^{CO} for $Ag_{(147-n)}Cys_n$ models were estimated from the DFT binding energies of ΔE_B^{COOH} and ΔE_B^{CO} using the fitted relationship between ΔG_B and ΔE_B empirically derived from the previous study of the ref 10. For comparison, ΔG_B^{COOH} and ΔG_B^{CO} calculated for (111) slab surface of Cu, Au, Ag, and Zn are also displayed, which well explains the experimental CO_2 reduction potential of metal foil.

cysteamine coverage increases up to 261 meV as the cysteamine/Ag ratio increases until 2.7%. Although it is difficult to experimentally quantify and/or control the cysteamine coverage to the Ag nanoparticles, we conceive that our 5 nm sized Ag/C sample have an optimal activity due to suitable coverage of anchoring agent, which was responsible for the remarkable reduction of overpotential. More interestingly, we found that the binding energy of the CO shows marginal changes with respect to the effect of anchoring agent. We note that modifying the catalyst surface to preferentially stabilize the intermediate (COOH) over the final product (CO) has its own importance in enhancing the catalytic activity.[10,25]

To find the mechanistic origin of the selective modulation of the surface binding energies for different adsorbates, we analyzed the electronic structure of cysteamine covered Ag

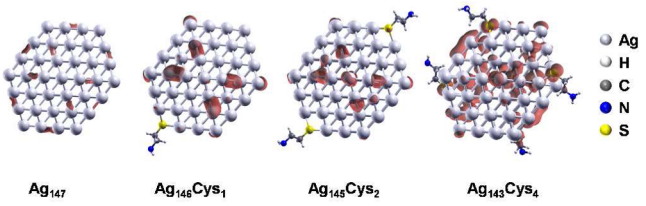

Figure 5. Electron spin density computed from DFT wave function is shown with the isosurface value of 0.001. Specific interaction developed in between Ag nanoparticle and the anchoring agents (cysteamine) leads the unpaired electron to be localized at the surface state of Ag nanoparticle, which helps to selectively stabilize COOH over CO.

nanoparticles. Figure 5 shows the change of spatial spin density of the Ag nanoparticles as the number of cysteamine increases (isosurface value is set as 0.001). In the context of superatom complex model,[26,27] $Ag_{(147-n)}Cys_n$ system can be understood as a superatom consisting of single unpaired electron. When no anchoring agent exists, this unpaired electron is delocalized over the entire superatom, which is too stable to be utilized for the chemical bonding with COOH radical. However, when anchoring agents are introduced, symmetry breaking leads to spatial localization of the unpaired electron particularly at the surface of Ag superatom (Figure 5). This can provide more covalent character to the Ag-COOH bond, which effectively stabilizes the intermediate (COOH radical). However, the localized unpaired electron is less effective in stabilizing the donor–acceptor bond between Ag and CO, resulting in a marginal change of the binding energy of CO. It is thus of noted that the effect of cysteamine can be understood using the previously suggested concept of covalency-aided electrochemical reaction (CAER) mechanism.[10]

■ CONCLUSION

In summary, silver nanoparticles with three different sizes were directly synthesized on a carbon support by a facile one-pot method using cysteamine as an anchoring agent, which initiated the nucleation on the carbon support. These novel nanoparticulate Ag/C samples were effective as electrocatalysts for the CO_2 reduction reaction in an aqueous system, and $^{13}CO_2$ isotope experiment confirmed that CO_2 was the carbon source to produce CO. Catalysts with 5 nm Ag/C sample exhibited the highest CO_2 reduction reaction activity in terms of low overpotential, high mass activity, high CO Faradaic efficiency, and high exchange current density with the enhanced durability. Significant reduction of the overpotential with directly grown Ag nanoparticle on carbon support was associated with the cysteamine anchoring agent, which developed Ag–S interaction. Our DFT studies elucidated that the Ag–S interaction induces surface localization of the unpaired electron, resulting in an enhanced intermediate stabilization and thus improved catalytic activity. These studies demonstrate the potential for using supported Ag nanoparticles synthesized by simple wet chemistry methods as CO_2 reduction catalysts with high mass activities and low overpotential for CO production and also suggest that anchoring groups such as cysteamine can be used to control their materials properties.

■ EXPERIMENTAL SECTION

Synthesis and Characterization of Ag Nanoparticles on Carbon Supports. For Ag nanoparticle/C, 20 mg of silver nitrate ($AgNO_3$; Aldrich, 99.9999%) was dissolved in 10 mL of ethylene

DOI: 10.1021/jacs.5b06568
J. Am. Chem. Soc. 2015, 137, 13844–13850

glycol (EG; Aldrich, 99.8%) with vigorous stirring and this solution was slowly heated to 50 °C for 20 min. Twenty mg of carbon black (Ketjen black) was dispersed in 10 mL EG and 1 mg of cysteamine solution (Aldrich) by ultrasonication for 30 min. Cysteamine was used as an anchoring agent. The prepared carbon black solution was added to the silver precursor solution at 50 °C, and the mixed solution was kept at 50 °C for 10 min prior to heating to 160 °C with a ramping rate of 3−4 °C/min. Three nm Ag/C and 5 nm Ag/C were synthesized by controlling the maintaining time at 160 °C for 1 and 3 h, respectively. For 10 nm Ag/C, 20 mg of silver acetylacetonate (Ag(acac); Aldrich, 98%) was dissolved in 10 mL 1-octadecene (ODE, Aldrich) under a nitrogen flow with vigorous stirring. The procedure was the same with the method above. The cysteamine-treatment carbon (denoted as Cysteamine-C) was prepared without Ag precursor following the same procedure.

The product solution was cooled down to room temperature, washed with isopropanol, filtered and dried. The prepared catalysts were analyzed by X-ray photoelectron spectroscopy (XPS; Thermo Scientific K-Alpha), X-ray diffraction (XRD; Shimadzu XRD-6000), inductively coupled plasma optical emission spectrometry (ICP-OES; Thermo Scientific iCAP 6300 Duo), transmission electron microscopy (TEM; TECNAI F20 G^2 at 200 kV) and high resolution transmission electron microscopy (HR-TEM; JEM-ARM200F at 200 kV).

Preparation of Working Electrode. The catalysts were dispersed into a mixture of isopropanol and Nafion solution (5 wt %, DuPont) to prepare a catalyst ink by sonication for 30 min. The actual metal amount in the solution was measured by inductively coupled plasma (ICP) elemental analysis. Glassy carbon plate (Alfa Aesar) was used as the electrode substrate after mechanically polishing and complete cleaning with deionized water. The catalyst ink solution was sprayed onto the glassy carbon plate. The active area of the electrode was 0.5 cm^2 and the sprayed amount of the metal catalyst was 0.09 ± 0.01 mg_{Ag}/cm^2.

The carbon and Cysteamine-C ink solutions were prepared by the same procedure and sprayed on the glassy carbon plate. For the comparison, Ag foil was used as a working electrode after mechanically polishing the surface, which electrode active area was also 0.5 cm^2.

Electrochemical Measurements. Platinum and Ag/AgCl (saturated KCl) were used as the counter electrode and the reference electrode, respectively. Electrochemical measurements were performed by using Ivium potentiostat (Iviumtechnology) in a two-compartment electrochemical cell, and a Nafion 117, a proton exchange membrane, was used to separate the catholyte and the anolyte. The electrolyte solution (0.5 M $KHCO_3$) was purged with high purity CO_2 gas for at least 1 h, where the pH was 7.0 after saturation. For obtaining stable electrochemical signals, chronoamperometry was performed at −2.0 V (vs Ag/AgCl) for 10 min prior to CO_2 reduction reaction measurements. The CO_2 reduction reaction were measured by using chronoamperometry at each fixed potential and gaseous products (i.e., H_2 and CO) were quantified by a gas chromatography (GC; Younglin 6500 GC) equipped with a pulsed discharge detector (PDD). Ultra high purity helium (He; 99.9999%) was used as the carrier gas. CO_2 average flow rate (Q) was 120 cc/min measured by a universal flow meter (Agilent technologies ADM 2000) at the exit of the electrochemical cell. The partial current and Faradaic efficiency of H_2 or CO production ($i_{H_2 \text{ or } CO}$ and $FE_{H_2 \text{ or } CO}$) were calculated from GC chromatogram peak areas where $V_{H_2 \text{ or } CO}$ is volume concentration of H_2 or CO based on calibration of the GC, i_{total} is measured current, F is Faradaic constant, p_0 is pressure, T is temperature, and R is ideal gas constant, 8.314 J·mol·K^{-1}.[11,28]

$$i_{H_2 \text{ or } CO} = V_{H_2 \text{ or } CO} \times Q \times \frac{2Fp_0}{RT}$$

$$FE_{H_2 \text{ or } CO} = \frac{i_{H_2 \text{ or } CO}}{i_{total}} \times 100$$

A durability test was performed for 5 h in CO_2-saturated 0.5 M $KHCO_3$ solution by chronoamperometry at a fixed potential that produced the highest Faradaic efficiency.

Solution resistance was obtained by measuring the electrochemical impedance spectroscopy (EIS) at various potential. The measured potentials for CO_2 reduction reaction were compensated for iR loss, and were reported versus the reversible hydrogen electrode (RHE) by using the following equation.

$$E(\text{vs RHE}) = E(\text{vs Ag/AgCl}) + 0.197V + 0.0591V \times \text{pH}$$

Density Functional Theory Calculations. Density functional theory (DFT) calculations were performed using Spanish Initiative for Electronic Simulations with Thousands of Atoms (SIESTA) program.[29,30] We chose exchange-correlation functional of Perdew−Burke−Ernzerhof (PBE) method,[31] and double-ζ level of basis sets were employed. For the sampling of reciprocal space, only the gamma point is sampled because we are considering the nonperiodic nanoparticles, and Mesh cutoff energy and force tolerance were set as 250 Ry and 0.1 eV/Å, respectively, for the geometry optimization.

■ ASSOCIATED CONTENT

Supporting Information

The Supporting Information is available free of charge on the ACS Publications website at DOI: 10.1021/jacs.5b06568.

Additional TEM image, XRD, and XPS spectra. Further electrocatalytic CO_2 reduction data with error bars. (PDF)

■ AUTHOR INFORMATION

Corresponding Authors

*bkmin@kist.re.kr

*yjhwang@kist.re.kr

Author Contributions

[▽]C.K. and H.S.J. contributed equally to this work.

Notes

The authors declare no competing financial interest.

■ ACKNOWLEDGMENTS

This work was supported by the program of the Korea Institute of Science and Technology (KIST) and University-Institute cooperation program of the National Research Foundation of Korea, funded by the Korean Government (MSIP). We also thank Young Scientists Fellowship program of National Research council of Science & Technology and the Rowland Institute at Harvard University for support through a Rowland Visiting Scholar Award.

■ REFERENCES

(1) Turner, J. A. *Science* **1999**, *285*, 687−689.

(2) Goeppert, A.; Czaun, M.; May, R. B.; Prakash, G. K. S.; Olah, G. A.; Narayanan, S. R. *J. Am. Chem. Soc.* **2011**, *133*, 20164−20167.

(3) Graves, C.; Ebbesen, S. D.; Mogensen, M.; Lackner, K. S. *Renewable Sustainable Energy Rev.* **2011**, *15*, 1−23.

(4) Centi, G.; Quadrelli, E. A.; Perathoner, S. *Energy Environ. Sci.* **2013**, *6*, 1711−1731.

(5) Mikkelsen, M.; Jorgensen, M.; Krebs, F. C. *Energy Environ. Sci.* **2010**, *3*, 43−81.

(6) Whipple, D. T.; Kenis, P. J. A. *J. Phys. Chem. Lett.* **2010**, *1*, 3451−3458.

(7) Hori, Y. In *Modern Aspects of Electrochemistry*; Vayenas, C., White, R., Gamboa-Aldeco, M., Eds.; Springer: New York, 2008; Vol. *42*, pp 89−189.

(8) Hatsukade, T.; Kuhl, K. P.; Cave, E. R.; Abram, D. N.; Jaramillo, T. F. *Phys. Chem. Chem. Phys.* **2014**, *16*, 13814−13819.

(9) Salehi-Khojin, A.; Jhong, H.-R. M.; Rosen, B. A.; Zhu, W.; Ma, S.; Kenis, P. J. A.; Masel, R. I. *J. Phys. Chem. C* **2012**, *117*, 1627−1632.

(10) Lim, H.-K.; Shin, H.; Goddard, W. A.; Hwang, Y. J.; Min, B. K.; Kim, H. *J. Am. Chem. Soc.* **2014**, *136*, 11355−11361.

DOI: 10.1021/jacs.5b06568
J. Am. Chem. Soc. 2015, 137, 13844−13850

(11) Chen, Y.; Li, C. W.; Kanan, M. W. *J. Am. Chem. Soc.* **2012**, *134*, 19969−19972.
(12) Lu, Q.; Rosen, J.; Zhou, Y.; Hutchings, G. S.; Kimmel, Y. C.; Chen, J. G.; Jiao, F. *Nat. Commun.* **2014**, *5*, 6.
(13) Zhu, W.; Michalsky, R.; Metin, Ö.; Lv, H.; Guo, S.; Wright, C. J.; Sun, X.; Peterson, A. A.; Sun, S. *J. Am. Chem. Soc.* **2013**, *135*, 16833−16836.
(14) Reske, R.; Mistry, H.; Behafarid, F.; Roldan Cuenya, B.; Strasser, P. *J. Am. Chem. Soc.* **2014**, *136*, 6978−6986.
(15) Zhu, W.; Zhang, Y.-J.; Zhang, H.; Lv, H.; Li, Q.; Michalsky, R.; Peterson, A. A.; Sun, S. *J. Am. Chem. Soc.* **2014**, *136*, 16132−16135.
(16) Zhang, J.; Liu, H.; Wang, Z.; Ming, N. *Adv. Funct. Mater.* **2007**, *17*, 3295−3303.
(17) Wang, C.; Daimon, H.; Onodera, T.; Koda, T.; Sun, S. *Angew. Chem., Int. Ed.* **2008**, *47*, 3588−3591.
(18) Grass, M. E.; Joo, S. H.; Zhang, Y.; Somorjai, G. A. *J. Phys. Chem. C* **2009**, *113*, 8616−8623.
(19) Kim, C.; Oh, J.-G.; Kim, Y.-T.; Kim, H.; Lee, H. *Electrochem. Commun.* **2010**, *12*, 1596−1599.
(20) Kim, C.; Kim, S. S.; Yang, S.; Han, J. W.; Lee, H. *Chem. Commun.* **2012**, *48*, 6396−6398.
(21) Kim, C.; Kim, J.; Yang, S.; Lee, H. *RSC Adv.* **2014**, *4*, 63677−63680.
(22) Battocchio, C.; Fratoddi, I.; Fontana, L.; Bodo, E.; Porcaro, F.; Meneghini, C.; Pis, I.; Nappini, S.; Mobilio, S.; Russo, M. V.; Polzonetti, G. *Phys. Chem. Chem. Phys.* **2014**, *16*, 11719−11728.
(23) Lee, J.-S.; Park, G. S.; Kim, S. T.; Liu, M.; Cho, J. *Angew. Chem., Int. Ed.* **2013**, *52*, 1026−1030.
(24) Gao, D.; Zhou, H.; Wang, J.; Miao, S.; Yang, F.; Wang, G.; Wang, J.; Bao, X. *J. Am. Chem. Soc.* **2015**, *137*, 4288−4291.
(25) Hansen, H. A.; Varley, J. B.; Peterson, A. A.; Nørskov, J. K. *J. Phys. Chem. Lett.* **2013**, *4*, 388−392.
(26) Hakkinen, H. *Chem. Soc. Rev.* **2008**, *37*, 1847−1859.
(27) Walter, M.; Akola, J.; Lopez-Acevedo, O.; Jadzinsky, P. D.; Calero, G.; Ackerson, C. J.; Whetten, R. L.; Grönbeck, H.; Häkkinen, H. *Proc. Natl. Acad. Sci. U. S. A.* **2008**, *105*, 9157−9162.
(28) Jeon, H. S.; Koh, J. H.; Park, S. J.; Jee, M. S.; Ko, D.-H.; Hwang, Y. J.; Min, B. K. *J. Mater. Chem. A* **2015**, *3*, 5835−5842.
(29) Ordejon, P.; Artacho, E.; Soler, J. M. *Phys. Rev. B: Condens. Matter Mater. Phys.* **1996**, *53*, 10441−10444.
(30) Soler, J. M.; Artacho, E.; Gale, J. D.; Garcia, A.; Junquera, J.; Ordejon, P.; Sanchez-Portal, D. *J. Phys.: Condens. Matter* **2002**, *14*, 2745−2779.
(31) Perdew, J. P.; Burke, K.; Ernzerhof, M. *Phys. Rev. Lett.* **1996**, *77*, 3865−3868.

DOI: 10.1021/jacs.5b06568
J. Am. Chem. Soc. 2015, 137, 13844−13850